Dependence of Raman and Resonance Raman Intensities on Sample Self-Absorption

Zhenmin Hong, Sanford A. Asher*

Department of Chemistry, University of Pittsburgh, 219 Parkman Ave., Pittsburgh, PA 15260 USA

Resonance Raman cross sections are generally larger than normal or preresonance Raman cross sections. Thus, higher Raman intensities are expected for resonance excitation, especially for backscattering measurements. However, self absorption decreases the observed Raman intensities. In the work here we examine the effect of self absorption on the observed preresonance and resonance Raman intensities. For the simplest case where a single electronic transition dominates the Raman scattering, and where the resonance enhancement scales with the square of the molar absorptivity of the absorption band, theory predicts that for close to resonance excitation the observed Raman intensities monotonically increase as resonance is approached. In the case that an impurity absorbs, the observed Raman intensities may decrease as excitation moves close to resonance for particular conditions of impurity absorption band widths and frequency offsets. Impurity absorption also causes decreases in observed Raman intensities for the more slowly increasing preresonance excitation.

Index Headings: **Raman; Resonance Raman; Self absorption; Standoff detection.**

INTRODUCTION

Raman spectroscopy involves inelastic light scattering.[1–3] The scattered light is collected using a collection optic, and this scattered light is then spectrally interrogated for its intensity, frequency, and polarization to get molecular information on the sample. The vibrational Raman scattering efficiency is generally low with normal analyte Raman cross sections of $\sim 10^{-30}$ cm^2 · molc^{-1} · str^{-1}. The cross sections will significantly increase if there is preresonance Raman enhancement; much larger Raman cross sections can occur with resonance excitation, especially in the deep ultraviolet (UV).[3,4] The largest resonance Raman cross sections observed to date are for polycyclic aromatic hydrocarbons such as pyrene, where cross sections as large as $\sim 10^{-22}$ cm^2 · molc^{-1} · str^{-1} occur.[5]

The Raman intensities observed depend upon the values of the Raman cross sections. However, the intensities observed are dramatically affected by phenomena such as sample self absorption that determines the depth of penetration of the excitation beam and the transmission of the Raman scattering out of the sample.[6–8]

Typical absorption cross sections are far larger ($\sim 10^{-16}$ cm^2 · molc^{-1}) than Raman cross sections, and even resonance Raman cross sections. For strong absorptions the excitation light is attenuated by the sample such that the sample thickness traversed can be limited to only tens of nanometers, limiting the number of Raman photons generated and observed. Attenuation of the incident light, as well as the Raman scattered light, can also result from sample elastic scattering due to the refractive index inhomogeneities that scatter the light outside of the volume elements that can be imaged into the spectrometer. These phenomena can significantly decrease the observed Raman intensities, which decrease the resulting spectral signal-to-noise ratio (S/N). Modern spectrometers use charge-coupled device (CCD) detectors. The Raman S/N in this case is limited by shot-noise and is proportional to the square root of the observed Raman intensities. Thus, the magnitude of the observed Raman intensities directly determines the Raman spectral S/N.

The affect of sample self absorption on the observed Raman intensities has previously been considered. For example, Strekas et al. examined the impact of self absorption on Raman intensities for a 90° scattering geometry,[7] while the 180° backscattering case was considered by Shriver and Dunn.[6] Greek et al. examined self absorption for the case of fiber optic measurements with a purpose of determining the optimal excitation wavelength.[9,10]

The Raman excitation profiles (REP) indicate the Raman cross section dependencies on excitation frequency.[11] The excitation frequency dependencies of the observed Raman intensities (EFDORI) have an additional large dependence on experimental parameters, especially the sample self absorption that is excitation frequency dependent.

We examine EFDORI in the simplest case (of pure samples) where a single resonant electronic transition dominates both the Raman scattering as well as the sample absorbance. In this case we show for the lowest order in theory that the EFDORI are expected to approximately follow the absorption band shape for optically thick samples. Thus, the maximum Raman spectral S/N measurement will occur for excitation at the maximum of the resonance REP, which generally occurs close to the absorption maximum for molecules with a single electronic transition.

In contrast, if additional absorption bands occur, from impurities or chromophores of the molecule not involved in the resonance Raman enhancement of a particular vibrational mode, these additional absorptions will attenuate the Raman intensities, leading to decreased S/N measurements. Depending on the particular conditions, preresonance Raman measurements can show

Received 24 March 2014; accepted 3 June 2014.

* Author to whom correspondence should be sent. E-mail: asher@pitt.edu.

DOI: 10.1366/14-07531

0003-7028/15/6901-0075/0

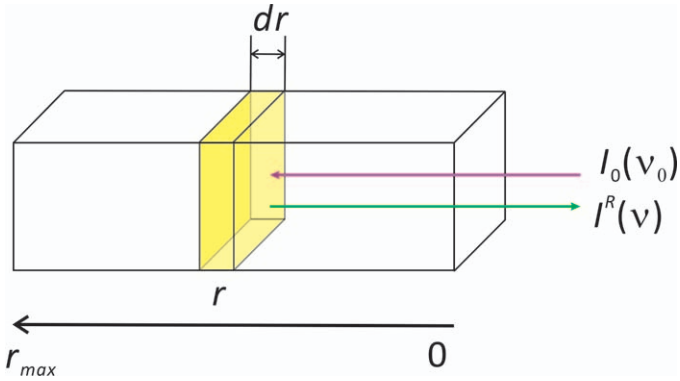

FIG. 1. Raman backscattering geometry.

higher intensities and S/N than resonance Raman measurements.

RESULTS AND DISCUSSION

Dependence of Resonance Raman Intensities on Self Absorption. We assume that all the Raman intensities derive solely from preresonance or resonance excitation from a single dominating electronic transition. We consider a simple backscattering geometry (Fig. 1) similar to that previously considered by Shriver and Dunn[6] where an incident excitation beam excites an extended planar sample normal to its surface. For simplicity we assume that we collect the Raman scattering only in the directly backscattered direction. This decreases the self absorption attenuation of the Raman backscattered light at angles $<180°$, because it neglects the longer path lengths traversed by this Raman scattering. In practice, a finite solid angle of Raman scattered light exiting the sample is collected over the finite depth of focus. This light is then focused onto the entrance slit with a complex transfer function. The light traverses and is dispersed using the spectrometer and is detected using the CCD.

Consider a volume element at depth r from the flat sample surface of thickness dr excited using a laser beam of frequency ν_0 with an illuminated cross sectional area of A. The Raman light scattered by this volume element is imaged into a Raman spectrometer and spectrally dispersed and detected. The backscattered Raman intensity observed at frequency ν is

$$dI^{R}_{ob}(r,\nu_0,\nu) \sim I_0(r,\nu_0)\cdot\sigma(\nu_0,\nu)\cdot c\cdot N_A\cdot\frac{\theta}{4\pi}\cdot K \cdot F\Big(\nu_0,\nu,r,\varepsilon(\nu_0),\varepsilon(\nu)\Big)\cdot A\cdot dr \quad (1)$$

where $I_0(r, \nu_0)$ is the incident excitation beam intensity at r, $\sigma(\nu_0, \nu)$ is the absolute Raman scattering cross section excited at ν_0 for a Raman band that occurs at ν, c is the analyte concentration, N_A is Avogadro's number, θ is the solid angle of the Raman scattered intensity collected using the spectrometer, K is the spectrometer efficiency, and $F(\nu_0, \nu, r, \varepsilon(\nu_0), \varepsilon(\nu))$ is the attenuation factor at the excitation and the Raman scattered light frequencies. For samples that do not elastically scatter light due to refractive index inhomogeneities, this factor results solely from absorption by the sample. The effective molar absorptivities at the excitation and Raman scattered frequencies are $\varepsilon(\nu_0)$ and $\varepsilon(\nu)$.

The exciting light is attenuated as

$$I(r,\nu_0) = I_0(\nu_0)\cdot e^{-2.303\cdot\varepsilon(\nu_0)\cdot c\cdot r} \quad (2)$$

The backscattering Raman light is attenuated by its transmission through the distance r through the sample:

$$dI^{R}_{ob}(r,\nu_0,\nu) = dI^{R}(r,\nu_0,\nu)\cdot e^{-2.303\cdot\varepsilon(\nu)\cdot c\cdot r} \quad (3)$$

where $dI^R(r, \nu_0, \nu)$ is the backscattered Raman intensity generated at position r in the sample. Thus, the attenuation factor for the contribution of a volume element at depth r is

$$F\Big(\nu_0,\nu,r,\varepsilon(\nu_0),\varepsilon(\nu)\Big) = e^{-2.303\cdot(\varepsilon(\nu_0)+\varepsilon(\nu))\cdot c\cdot r} \quad (4)$$

Therefore, the total Raman intensity detected is the integral of $dI^{R}_{ob}(r, \nu_0, \nu)$ over the sample thickness illuminated using the incident excitation beam:

$$\begin{aligned} I^{R}_{ob}(\nu_0,\nu) &\sim \int_0^{r_{max}} dI^{R}_{ob}(r,\nu_0,\nu)\,dr \\ &= I_0(\nu_0)\cdot A\cdot\sigma(\nu_0,\nu)\cdot c\cdot N_A\cdot\frac{\theta}{4\pi}\cdot K \\ &\quad\cdot\int_0^{r_{max}} e^{-2.303\cdot(\varepsilon(\nu_0)+\varepsilon(\nu))\cdot c\cdot r}\,dr \end{aligned} \quad (5)$$

For a sample of thickness r_{max},

$$I^{R}_{ob}(\nu_0,\nu) \sim \frac{I_0(\nu_0)\cdot A\cdot\sigma(\nu_0,\nu)\cdot N_A\cdot\theta\cdot K}{2.303\cdot 4\pi\cdot\Big(\varepsilon(\nu_0)+\varepsilon(\nu)\Big)}\cdot\Big(1-e^{-2.303\cdot(\varepsilon(\nu_0)+\varepsilon(\nu))\cdot c\cdot r_{max}}\Big) \quad (6)$$

The observed Raman intensity increases with the Raman cross section and decreases with the absorbance at the excitation and Raman scattering frequencies. The Raman intensities observed are relatively independent of concentration[6] but are decreased for sample thicknesses less than that necessary to fully attenuate the excitation beam.

The Raman scattering cross sections are proportional to the fourth power of the excitation frequency times the square of Raman polarizability:[12]

$$\sigma(\nu_0,\nu) \sim \nu_0^4|\alpha(\nu_0,\nu)|^2 \quad (7)$$

With Kramer–Heisenberg–Dirac second order perturbation theory, we can write down an expression for the resonance Raman polarizability in the lowest order in Raman theory as detailed through the Albrecht A term expression:[12]

$$\alpha(\nu_0,\nu) \sim <g|\mu|e><e|\mu|g>\cdot FC\cdot D(\nu_e,\nu_0,\nu) \quad (8)$$

where the transition moment integrals occur over the electric dipole operator, μ, between the electronic

ground state and the resonant electronic excited state. FC is the factor associated with the Franck–Condon integrals for the vibrational mode selection factor of the Raman polarizability, while $D(\nu_e, \nu_0, \nu)$ is the resonant excitation energy denominator that determines the dispersion of the Raman cross section due to preresonance and resonance effects.

The square of the electronic transition moment is roughly *proportional* to the maximum molar absorptivity, $\varepsilon(\nu_e)$, where ν_e is the frequency at which the electronic transition occurs. Thus, the resonance Raman cross section for the vibration that scatters at frequency ν is proportional to the square of the molar absorptivity.[12] In this regard Tuschel et al. recently showed that the 229 nm excited resonance Raman scattering cross sections of a number of explosives are proportional to the square of their 229 nm absorbances.[13]

$$\sigma(\nu_0) \sim k \cdot \nu_0^4 \cdot \varepsilon^2(\nu_0) \tag{9}$$

In strict resonance, the REP will approximately track the absorption band shape if the absorption is dominated by inhomogeneous broadening. In this case the absorption band shape results from a set of molecules with a distribution of transition frequencies. The resonance REP results from the sum of the contributions of the individual REP contributed by each of these transitions.

If the absorption band shape is dominated by homogeneous broadening, the relationship between the absorption band shape and the resonance REP becomes somewhat more complex. However, the following conclusions are expected to approximately hold for this case as well.

By approximating $\varepsilon(\nu_0) = \varepsilon(\nu)$ (for deep UV Raman excitation, the Stokes shift frequency is small compared to the excitation frequency), we can simplify Eq. 6,

$$I_{ob}^{R}(\nu_0) \sim \frac{k \cdot I_0(\nu_0) \cdot \nu_0^4 \cdot \varepsilon^2(\nu_0) \cdot A \cdot N_A \cdot \theta \cdot K}{4.606 \cdot 4\pi \cdot \varepsilon(\nu_0)} \cdot \left(1 - e^{-4.606 \cdot \varepsilon(\nu_0) \cdot c \cdot r_{max}}\right) \tag{10}$$

If the product of the molar absorptivity $\varepsilon(\nu_0)$, the concentration c, and the sample path length is large, the exponential term becomes zero. Equation 10 becomes

$$I_{ob}^{R}(\nu_0) \sim \frac{k \cdot I_0(\nu_0) \cdot \nu_0^4 \cdot \varepsilon(\nu_0) \cdot A \cdot N_A \cdot \theta \cdot K}{4.606 \cdot 4\pi} \tag{11}$$

This expression indicates that even in the presence of self absorption, the backscattered Raman intensities become proportional to the molar absorptivity $\varepsilon(\nu_0)$ and are independent of concentration. The EFDORI tracks the analyte absorption band shape but is biased to higher frequency by the ν_0^4 scattering dependence. The largest Raman intensities will occur at the absorption spectral maximum. Resonance Raman excitation will always give rise to higher intensities (and higher S/N) than will normal and preresonance Raman measurements.

This is the behavior expected from close to resonance excited Raman bands whose preresonance intensities are enhanced using a single electronic transition that is situated at higher frequency.

An example of this type of enhancement occurs for the symmetric NO_3^- stretch at ~1050 cm^{-1} in NH_4NO_3 and in $NaNO_3$, whose entire preresonance and resonance enhancement derives from its ~220 nm lowest energy absorption band.[13–15] In this case all of the absorption oscillator strength of molecule is located in the NO_3^- moiety in aqueous solution. Water and Na^+ and NH_4^+ counterion absorptions lie deeper in the UV and negligibly contribute for $\lambda_0 > 200$ nm.

If the self absorption is small (conditions where $\varepsilon(\nu_0) \cdot c \cdot r_{max}$ is small) we can expand the exponential term in Eq. 10 to obtain

$$I_{ob}^{R}(\nu_0) \sim \frac{\theta}{4\pi} k \cdot I_0(\nu_0) \cdot \nu_0^4 \cdot \varepsilon^2(\nu_0) \cdot A \cdot N_A \cdot K \cdot c \cdot r_{max} \tag{12}$$

In this case the backscattered Raman intensity more strongly increases with analyte absorption since it is proportional to $\varepsilon^2(\nu_0)$. Equation 12 indicates that the observed intensity increases with sample thickness and analyte concentration. This expression ignores the limitation in the observed intensity due to the collection optic finite depth of focus that limits the volume from which the Raman intensity can be collected.

Impact of Impurity Absorption on Raman Intensities. In this case, sample self absorption decreases the observed Raman intensities compared with the case above, where the single absorption band enhances the Raman intensities. This can be shown from Eq. 13, which explicitly includes an absorption band not involved in resonance Raman enhancement.

$$I_{obi}^{R}(\nu_0) \sim \frac{k \cdot I_0(\nu_0) \cdot \nu_0^4 \cdot \varepsilon_a^2(\nu_0) \cdot c_a \cdot A \cdot N_A \cdot \theta \cdot K}{4.606 \cdot 4\pi \cdot \left(\varepsilon_a(\nu_0) c_a + \varepsilon_i(\nu_0) c_i\right)} \cdot \left(1 - e^{-4.606(\varepsilon_a(\nu_0) c_a + \varepsilon_i(\nu_0) c_i) r_{max}}\right) \tag{13}$$

where ε_a and c_a are the molar absorptivity and the concentration of the analyte that is resonance enhanced and ε_i and c_i are the molar absorptivity and the concentration of an impurity or absorbing chromophore that does not enhance the analyte Raman bands. This additional absorption could include, for example, chromophores such as Cs^+ in solutions of $CsNO_3$. The NO_3^- in aqueous solution shows the same REP as occurs in the presence of the transparent NH_4^+ and Na^+ counterions. However, the Cs^+ absorption will attenuate the observed Raman intensities. The additional absorptions may also derive from impurities, or from other electronic transitions of a macromolecular analyte, or derive from photochemically generated impurities.

Equation 13 points out that for an optically thick sample the observed Raman intensity will be attenuated by

$$R = \frac{I_{obi}^{R}(\nu_0)}{I_{ob}^{R}(\nu_0)} = \frac{\varepsilon_a(\nu_0) c_a}{\varepsilon_a(\nu_0) c_a + \varepsilon_i(\nu_0) c_i} \tag{14}$$

where R is the ratio of the Raman intensities in the presence, $I_{obi}^{R}(\nu_0)$, and in the absence, $I_{ob}^{R}(\nu_0)$, of the

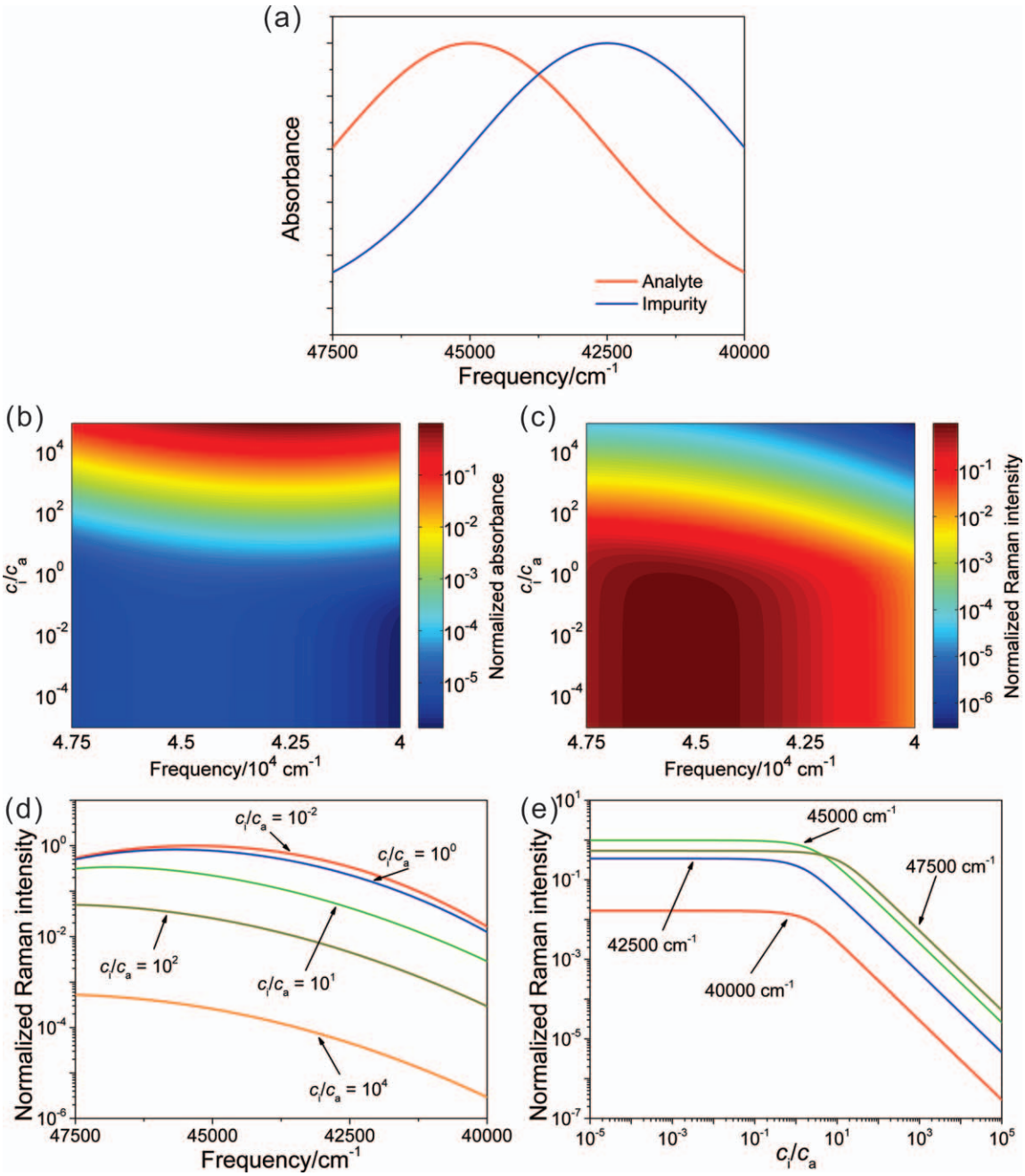

FIG. 2. (**a**) Analyte and impurity absorptions. The absorption bands are Gaussians, with $\sigma_a = \sigma_i = 2500\ cm^{-1}$, and with maxima at $\nu_{ac} = 45\ 000\ cm^{-1}$ and $\nu_{ic} = 42\ 500\ cm^{-1}$, respectively. (**b**) Contour plot of calculated frequency dependence of sample absorbance as a function of relative impurity concentration. The normalized absorbance is calculated by dividing by the maximum absorbance that occurs at the maximum impurity concentration of $c_i/c_a = 10^5$. (**c**) EFDORI as a function of the relative impurity concentration calculated using Eq. 13. The resonance Raman intensities are normalized to the maximum Raman intensity that occurs for $c_i/c_a = 10^{-5}$. (**d**) Calculated EFDORI at different relative impurity concentrations. (**e**) Relative impurity concentration dependence of Raman intensities.

impurity. It should be noted that the attenuation calculated is strictly for the case where the absorbing species are intimately intermixed with the analyte. It would not be valid for detection of surface analyte particles that are not subject to interferent absorptions.

Figure 2 shows the calculated sample absorbance and resonance Raman intensities as a function of frequency and relative impurity concentrations (c_i/c_a). Assuming that the impurity absorption has identical band shape and absorptivity as analyte absorption (Fig. 2a) at low impurity concentrations, the sample absorbance mainly derives from the analyte. As the impurity concentration increases, the absorbance becomes dominated by the impurity absorbance (Fig. 2b).

For all impurity concentrations, the EFDORI monotonically increases as the excitation frequencies move into resonance (Fig. 2c). There is no case where impurity absorption causes a dip in the EFDORI for this set of parameters. However, the Raman intensities do decrease as the impurity concentrations increase.

Figure 2d shows that the EFDORI maxima slightly shift toward higher frequencies because the increased

impurity absorbance (maximum at 42 500 cm^{-1}) attenuates the EFDORI on the low frequency side. Figure 2e shows the dependence of Raman intensity on the relative impurity concentration (c_i/c_a) at different excitation frequencies. At low impurity concentrations, the Raman intensity is little affected. The Raman intensities decrease as the impurity concentrations increase.

The approximation that the Raman cross section increases with the square of the molar absorptivity, which is relevant for true resonance excitation, predicts that the maximum intensities occur for resonance excitation. In most cases the square of the analyte absorption grows faster with frequency than does the sample absorption. The observed resonance Raman intensity increases with excitation frequency. In the rare cases we examine below, attenuation of the observed Raman intensities caused by impurity absorption could exceed the resonance enhancement and result in a dip in the EFDORI.

We should also mention that much more complex situations can occur for more complex samples. For example, analytes may have multiple absorption bands. In this case constructive and destructive interference can occur between different electronic transitions.[16,17] This can complicate the behavior of the REP, especially for excitation at frequencies between absorption bands.

Conditions in Which Sample Self Absorption Causes Excitation Frequency Dependencies of the Observed Raman Intensity Minima. Figure 2 demonstrates that the observed Raman intensities monotonically increase as the excitation frequency approaches resonance even in the presence of an absorbing impurity. For optically thick samples, the exponential term in Eq. 13 vanishes.

$$I^{R}_{obi}(\nu_0) \sim \frac{k \cdot I_0(\nu_0) \cdot \nu_0^4 \cdot \varepsilon_a(\nu_0)^2 \cdot c_a \cdot A \cdot N_A \cdot \theta \cdot K}{4.606 \cdot 4\pi \cdot \left(\varepsilon_a(\nu_0)c_a + \varepsilon_i(\nu_0)c_i\right)} \quad (15)$$

In general, the EFDORI monotonically increases as the excitation frequency is tuned into resonance due to its dependence on the molar absorptivity squared in the numerator as demonstrated in Fig. 2. However, it is possible to have situations where the impurity absorbs in such a way that the EFDORI decreases as the excitation frequency approaches resonance.

Below we determine the conditions for the presence of a minimum in the EFDORI. For simplicity we assume Gaussian absorption band shapes. This is also motivated by the fact that in the condensed phase, inhomogeneous broadening often dominates absorption band shapes.

$$\varepsilon_a(\nu_0) = \varepsilon_{ac} e^{-\frac{(\nu_0-\nu_{ac})^2}{2\sigma_a^2}} \quad (16)$$

$$\varepsilon_i(\nu_0) = \varepsilon_{ic} e^{-\frac{(\nu_0-\nu_{ic})^2}{2\sigma_i^2}} \quad (17)$$

where ε_{ac} and ε_{ic} are the analyte and impurity maximum molar absorptivities, ν_{ac} and ν_{ic} are the analyte and impurity absorption frequency maxima, and σ_a and σ_i are the analyte and impurity standard deviations of the Gaussian bands, respectively (not to be confused with the Raman scattering cross section σ).

We shall limit our discussion to the resonance excitation region in the case that the impurity absorption maximum occurs to lower frequency than the resonance absorption: $\nu_{ac} - 2\sigma_a \le \nu_0 \le \nu_{ic} \le \nu_{ac}$. Obviously, a minimum in the EFDORI requires $\varepsilon_i(\nu_0)c_i \gg \varepsilon_a(\nu_0)c_a$. We can rewrite Eq. 15 to concentrate on the absorption factors by substituting Eq. 16 and Eq. 17 into Eq. 15.

$$I^{R}_{obi}(\nu_0) \sim \frac{k \cdot I_0(\nu_0) \cdot \nu_0^4 \cdot \left(\varepsilon_{ac} e^{-\frac{(\nu_0-\nu_{ac})^2}{2\sigma_a^2}}\right)^2 \cdot c_a \cdot A \cdot N_A \cdot \theta \cdot K}{4.606 \cdot 4\pi \cdot c_i \cdot \varepsilon_{ic} \cdot e^{-\frac{(\nu_0-\nu_{ic})^2}{2\sigma_i^2}}} \quad (18)$$

In the UV region, $\nu_0 \gg \sigma_a$; therefore, the ν_0^4 factor changes little between $\nu_{ac} - 2\sigma_a$ and ν_{ac}, compared with the Gaussian factors. Thus, we conveniently ignore this variation and include the ν_0^4 factor in a constant K', which collects all constants and is independent on ν_0.

$$I^{R}_{obi}(\nu_0) \sim \frac{K' c_a \left(\varepsilon_{ac} e^{-\frac{(\nu_0-\nu_{ac})^2}{2\sigma_a^2}}\right)^2}{c_i \cdot \varepsilon_{ic} \cdot e^{-\frac{(\nu_0-\nu_{ic})^2}{2\sigma_i^2}}} \quad (19)$$

As the excitation frequency increases, a dip occurs in the EFDORI if the derivative of $I^{R}_{obi}(\nu_0)$ with respect to ν_0 becomes negative:

$$\frac{dI^{R}_{obi}(\nu_0)}{d\nu_0} = I^{R}_{obi}(\nu_0)\frac{d\ln I^{R}_{obi}(\nu_0)}{d\nu_0} < 0 \quad (20)$$

Since $I^{R}_{obi}(\nu_0) > 0$, Eq. 20 becomes

$$\frac{d\ln I^{R}_{obi}(\nu_0)}{d\nu_0} = -\frac{2(\nu_0-\nu_{ac})}{\sigma_a^2} + \frac{(\nu_0-\nu_{ic})}{\sigma_i^2} < 0 \quad (21)$$

Collecting terms and rearranging,

$$(\sigma_a^2 - 2\sigma_i^2)\nu_0 < \sigma_a^2\nu_{ic} - 2\sigma_i^2\nu_{ac} \quad (22)$$

We denote

$$\beta \equiv \frac{\sigma_i}{\sigma_a} \quad (23)$$

$$\lambda \equiv \frac{\nu_{ac}}{\sigma_a} \quad (24)$$

$$\delta \equiv \frac{\nu_{ac} - \nu_{ic}}{\sigma_a} = \lambda - \frac{\nu_{ic}}{\sigma_a} \quad (25)$$

Obviously $\beta > 0$, $\lambda > 0$, and $\delta \ge 0$. Using Eqs. 23–25, we further replace σ_i, ν_{ac}, and ν_{ic} with $\beta\sigma_a$, $\lambda\sigma_a$, and $(\lambda - \delta)\sigma_a$, respectively. Equation 22 becomes

$$(1 - 2\beta^2)\sigma_a^2\nu_0 < \sigma_a^2((\lambda - \delta)\sigma_a) - 2(\beta\sigma_a)^2\lambda\sigma_a \quad (26)$$

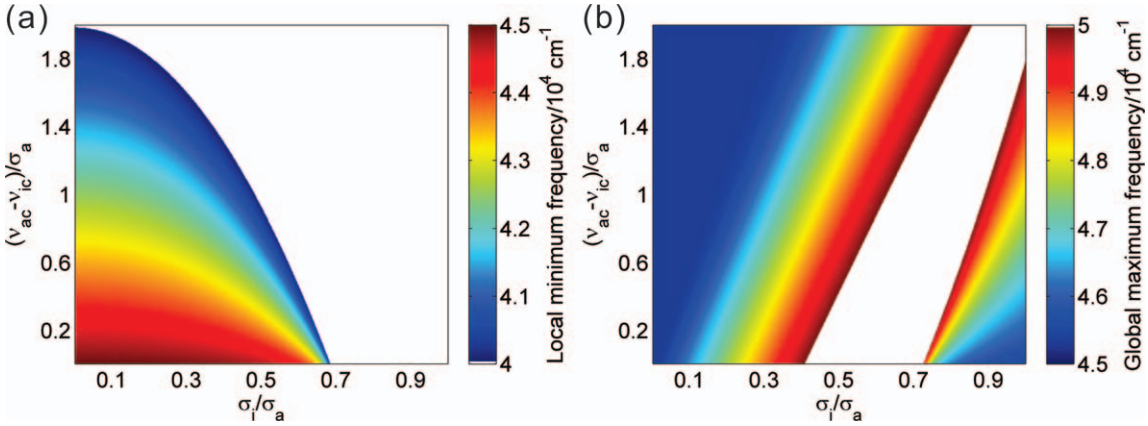

FIG. 3. (**a**) Dependencies of the EFDORI local minimum frequency on the relative absorption band widths (σ_i/σ_a) and absorption band maximum frequency offsets (($\nu_{ac}-\nu_{ic}$)/σ_a). (**b**) EFDORI maximum frequency dependence on relative absorption band widths (σ_i/σ_a) and absorption band maximum frequency offsets (($\nu_{ac}-\nu_{ic}$)/σ_a). The local minimum frequencies, local maximum frequencies, and resonance maximum frequencies are obtained from EFDORI that are calculated using Eq. 13 with $\nu_{ac} = 45\ 000\ cm^{-1}$, $\sigma_a = 2500\ cm^{-1}$, $c_i/c_a = 10^5$, and the corresponding δ and β. The blank regions indicate regions without minima or maxima in the domain of interest ([$\nu_{ac}-2\sigma_a$, $\nu_{ac}+2\sigma_a$]). The boundary in (**a**) is approximate, due to neglecting ν_0^4.

Canceling σ_a^2 on both sides and rearranging gives

$$(1-2\beta^2)\nu_0 < (\lambda-\delta)\sigma_a - 2\lambda\beta^2\sigma_a \tag{27}$$

If $(1-2\beta^2) > 0$, $0 < \beta < 1/(2^{1/2})$, then

$$\nu_0 < \frac{(\lambda-\delta)\sigma_a - 2\lambda\beta^2\sigma_a}{(1-2\beta^2)} \tag{28}$$

Since $\nu_{ac} - 2\sigma_a \le \nu_0$, the following must hold,

$$\nu_{ac} - 2\sigma_a = \lambda\sigma_a - 2\sigma_a < \frac{(\lambda-\delta)\sigma_a - 2\lambda\beta^2\sigma_a}{(1-2\beta^2)} \tag{29}$$

Multiplying both sides by $(1-2\beta^2)/\sigma_a$ and rearranging, we obtain $\delta < 2(1-2\beta^2)$. Since $\nu_0 \le \nu_{ic}$ and $\nu_0 < [(\lambda-\delta)\sigma_a - 2\lambda\beta^2\sigma_a]/(1-2\beta^2)$ (Eq. 29), we want to compare the values of $[(\lambda-\delta)\sigma_a - 2\lambda\beta^2\sigma_a]/(1-2\beta^2)$ and ν_{ic}, and choose the smaller quantity as the upper limit for ν_0. It can be shown that the following holds, because $\beta > 0$, $\delta \ge 0$.

$$\frac{(\lambda-\delta)\sigma_a - 2\lambda\beta^2\sigma_a}{(1-2\beta^2)} \le (\lambda-\delta)\sigma_a = \nu_{ic} \tag{30}$$

Therefore, $\nu_0 < [(\lambda-\delta)\sigma_a - 2\lambda\beta^2\sigma_a]/(1-2\beta^2) \le \nu_{ic}$.

In the case that $(1-2\beta^2)$, where $\beta > 1/(2^{1/2})$, Eq. 27 has a different solution,

$$\nu_0 > \frac{(\lambda-\delta)\sigma_a - 2\lambda\beta^2\sigma_a}{(1-2\beta^2)} \tag{31}$$

Since $\nu_0 \le \nu_{ic}$, together with Eq. 31 this leads to

$$\frac{(\lambda-\delta)\sigma_a - 2\lambda\beta^2\sigma_a}{(1-2\beta^2)} < \nu_0 \le \nu_{ic} = (\lambda-\delta)\sigma_a \tag{32}$$

Note $(1-2\beta^2) < 0$ in this case. Rearranging Eq. 32,

$$2\beta^2\delta < 0 \tag{33}$$

Obviously, Eq. 33 is not a relevant solution, because $\beta > 0$, $\delta \ge 0$.

Thus, we conclude that for the EFDORI to show a minimum caused by self absorption in the frequency range between $\nu_{ac} - 2\sigma_a$ and ν_{ac} requires

(1) The band width of the impurity absorption must be less than the resonant analyte absorption, $\sigma_i/\sigma_a < 1/(2^{1/2})$;
(2) The frequency difference between the analyte absorption maximum and the impurity absorbance maximum, $\nu_{ac} - \nu_{ic} \le 2\sigma_a(1-2(\sigma_i/\sigma_a)^2)$.

When these two requirements are satisfied, the observed Raman intensity minimum is expected at $\nu_0 = [(\lambda-\delta)\sigma_a - 2\lambda\beta^2\sigma_a]/(1-2\beta^2)$. Our neglect of the ν_0^4 dependence only causes small errors.

The above analysis considers only a single impurity absorption band. In the cases of multiple impurity absorptions, the overall impurity absorption band shape could deviate significantly from a Gaussian band shape. In this case, observation of a minimum in EFDORI still requires that the impurity absorption increases faster with frequency than does the Raman cross section.

Figure 3 displays the frequencies of minima (if any) in the EFDORI calculated from Eq. 13 above. Figure 3a shows blank areas above the line $(\nu_{ac}-\nu_{ic})/\sigma_a = 2(1-2(\sigma_i/\sigma_a)^2)$, where no minima occur over the range where Eq. 9 is valid. Below this boundary, the frequency of the EFDORI minimum decreases as the impurity absorption band broadens and as the impurity absorption band downshifts from the analyte absorption. Figure 3b shows the frequencies of the EFDORI maxima.

Figure 2 calculates the normalized Raman intensity at $\sigma_i/\sigma_a = 1$ and $(\nu_{ac}-\nu_{ic})/\sigma_a = 1$ and in a region where no local minima occur in the EFDORI. In contrast, Fig. 4 calculates the normalized Raman intensities where minima exist for $\sigma_i/\sigma_a = 0.2$ and $(\nu_{ac}-\nu_{ic})/\sigma_a = 0.6$.

The impurity absorption band shape is now much narrower than that of analyte absorption (Figs. 4a and 4b). As expected, low impurity concentrations have little

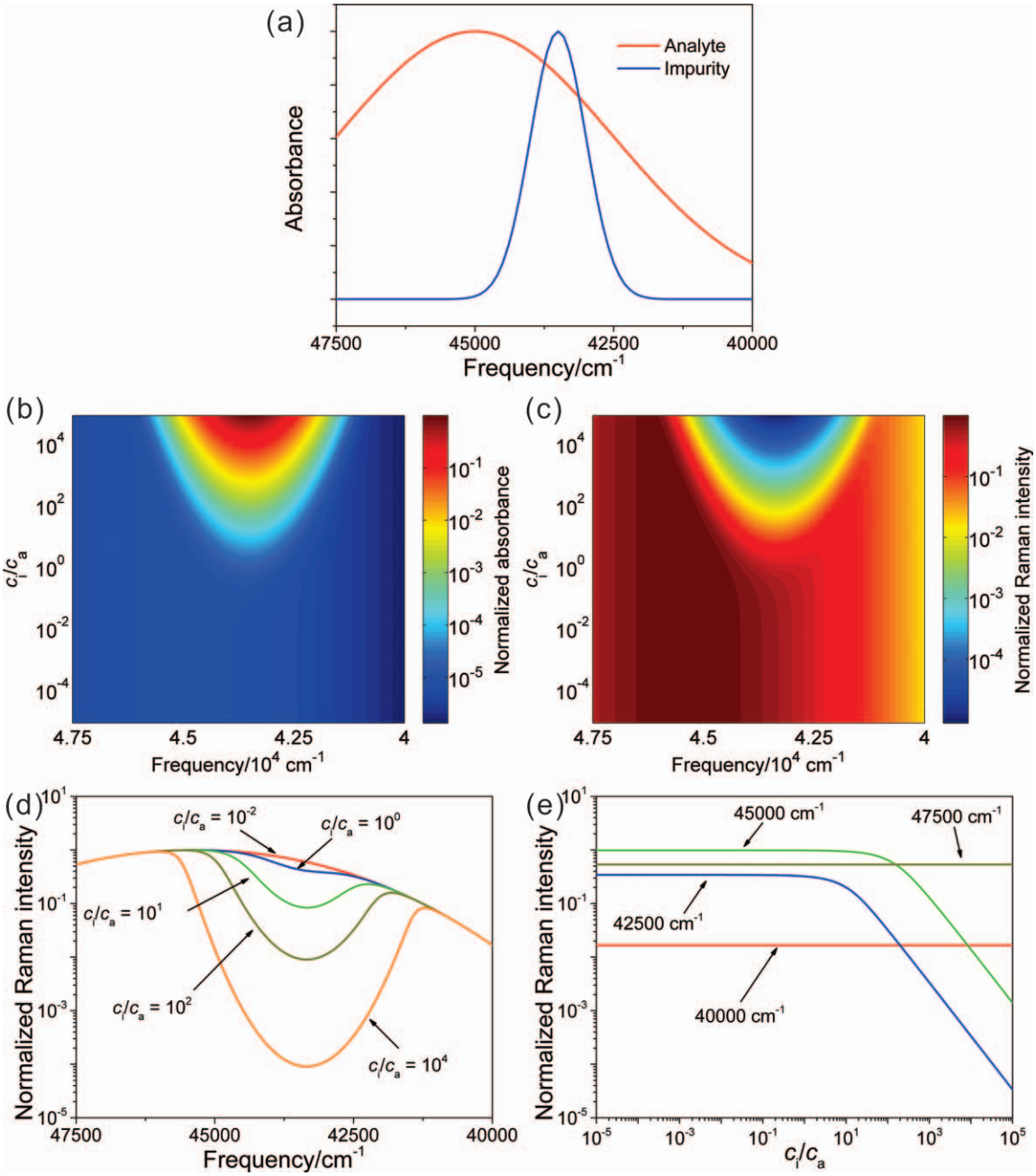

FIG. 4. (**a**) Analyte and impurity absorption spectra. The analyte absorption band maximum frequency is $\nu_{ac} = 45\ 000\ cm^{-1}$ with $\sigma_a = 2500\ cm^{-1}$. The impurity absorption band maximum frequency is $\nu_{ic} = 43\ 500\ cm^{-1}$ with $\sigma_i = 500\ cm^{-1}$. ($\sigma_i/\sigma_a = 0.2$, $(\nu_{ac} - \nu_{ic})/\sigma_a = 0.6$) (**b**) Contour plot of calculated frequency dependence of sample absorbance as a function of relative impurity concentrations. The normalized absorbance is calculated by dividing by the maximum absorbance that occurs at the maximum impurity concentration of $c_i/c_a = 10^5$. (**c**) Contour plot of the EFDORI as a function of the relative impurity concentration calculated from Eq. 13. The resonance Raman intensities are normalized to the maximum Raman intensity that occurs for $c_i/c_a = 10^{-5}$. (**d**) EFDORI at different relative impurity concentrations. (**e**) Relative impurity concentration dependence of observed Raman intensities.

impact on the observed Raman intensities. However, impurity concentrations comparable to or greater than the analyte give rise to EFDORI minima localized where the impurity has strong absorption (Figs. 4c and 4d). Beyond this frequency region, the observed Raman intensities are independent of impurity concentration (Fig. 4e).

Dependence of Preresonance Raman Intensities on Self Absorption. In the cases above we assumed that the resonance Raman enhancement scales with the square of the molar absorptivity. Thus, the Raman intensities will always be maximized with resonance excitation, unless the impurity absorbance increases faster than does the square of the analyte absorbance.

If the Raman intensities increase at a slower rate with excitation frequency, impurity absorption can dramatically impact the preresonance Raman intensities. This is the case where the preresonance Raman cross sections

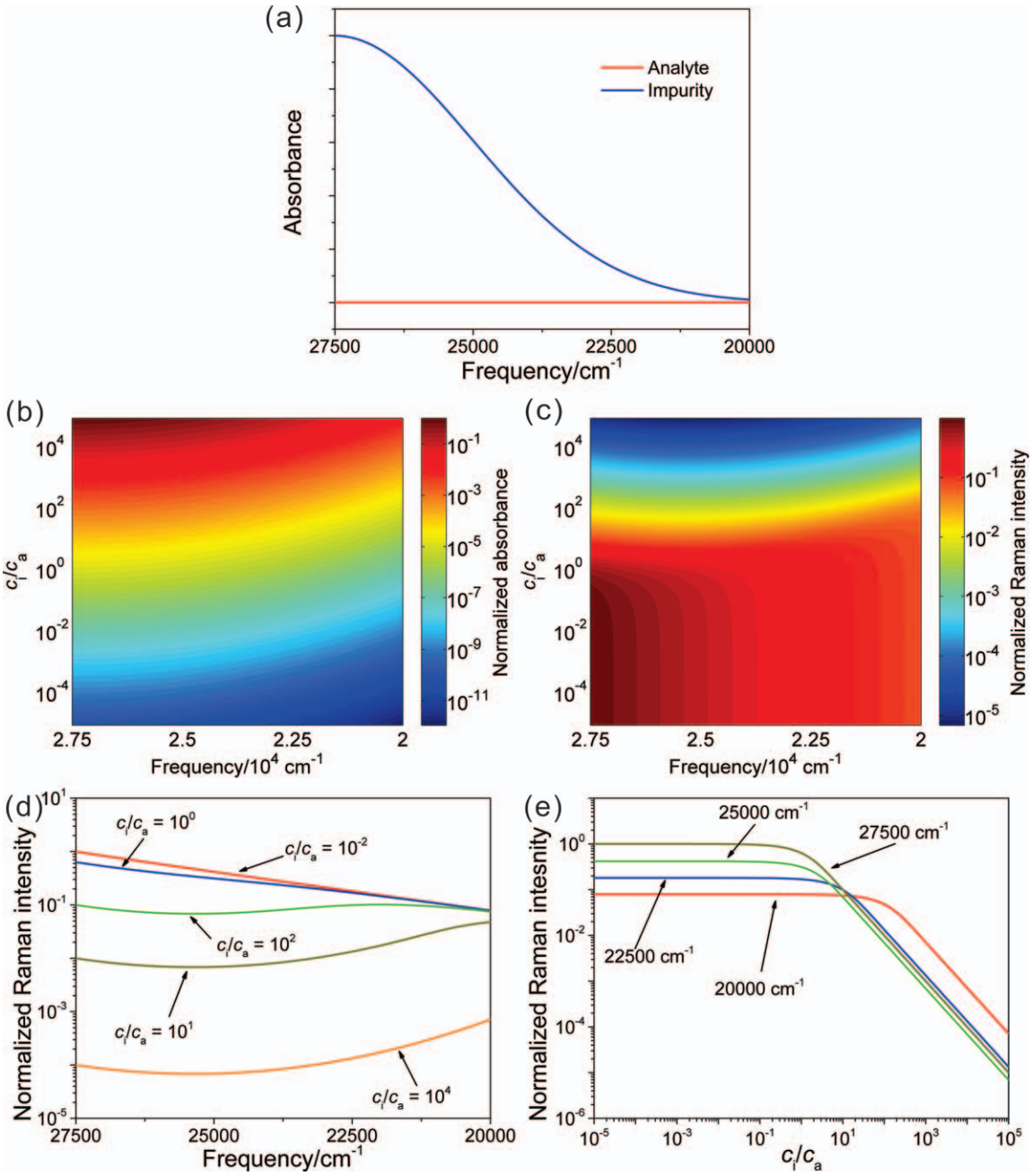

FIG. 5. (**a**) Analyte and impurity absorption spectra. The analyte and impurity absorption bands are Gaussians, with $\sigma_a = \sigma_i = 2500\ cm^{-1}$, and with maxima at $\nu_{ac} = 45\ 000\ cm^{-1}$ and $\nu_{ic} = 27\ 500\ cm^{-1}$, respectively. (**b**) Contour plot of calculated frequency dependence of sample absorbance as a function of relative impurity concentrations. The normalized absorbance is calculated by dividing by the maximum absorbance that occurs at the maximum impurity concentration of $c_i/c_a = 10^5$. (**c**) Observed contour plot of the EFDORI as a function of the relative impurity concentration calculated from Eq. 35. The preresonance Raman intensities are normalized to the maximum Raman intensity that occurs for $c_i/c_a = 10^{-5}$. (**d**) EFDORI at different relative impurity concentrations. (**e**) Relative impurity concentration dependence of observed preresonance Raman intensities.

follow the preresonance Raman Albrecht A term:

$$\sigma(\nu_0) \sim k'\nu_0^4 \left[\frac{\nu_e^2 + \nu_0^2}{(\nu_e^2 - \nu_0^2)^2}\right]^2 \tag{34}$$

where ν_0 is the excitation frequency, and ν_e is the frequency of the electronic transition giving rise to preresonance Raman enhancement. The ν_0 excited observed Raman intensity for a sample containing impurity absorption is

$$I_{obi}^{R}(\nu_0) \sim \frac{k' \cdot I_0(\nu_0) \cdot \nu_0^4 \left[\frac{\nu_e^2+\nu_0^2}{(\nu_e^2-\nu_0^2)^2}\right]^2 \cdot c_a \cdot A \cdot N_A \cdot \theta \cdot K}{4.606 \cdot 4\pi \cdot \varepsilon_i(\nu_0) c_i} \cdot \left(1 - e^{-4.606 \cdot \varepsilon_i(\nu_0) c_i r_{max}}\right) \tag{35}$$

In preresonance Raman the absorbance of the analyte is negligible. For optically thick samples, the exponential

term vanishes and Eq. 35 becomes

$$I^{R}_{obi}(\nu_0) \sim \frac{k' \cdot I_0(\nu_0) \cdot \nu_0^4 \left[\frac{\nu_e^2+\nu_0^2}{(\nu_e^2-\nu_0^2)^2}\right]^2 \cdot c_a \cdot A \cdot N_A \cdot \theta \cdot K}{4.606 \cdot 4\pi \cdot \varepsilon_i(\nu_0) c_i} \quad (36)$$

If we assume that the impurity absorption band is a Gaussian, we find cases where impurity absorption decreases the Raman intensities as the excitation frequency increases toward resonance.

Figure 5 shows the simulated sample absorbance and preresonance Raman intensities as a function of frequency and relative impurity concentration (c_i/c_a). The analyte shows little absorption in this frequency region (Fig. 5a). At very low impurity concentrations, the sample shows little absorption. At high impurity concentrations, it only shows impurity absorbance (Fig. 5b). With low impurity concentrations, the observed preresonance Raman intensities monotonically increase with excitation frequency (Figs. 5c and 5d). The rate is slower than in the resonance case. In contrast, at high impurity concentrations, the observed preresonance Raman intensities show minima at $\sim$26 000 cm^{-1} (Fig. 5d). The observed preresonance Raman intensities decrease as the impurity concentration increases (Fig. 5e).

CONCLUSIONS

We examined the impact of self absorption on the Raman intensity observed for a 180° backscattering geometry. In the absence of impurities, the observed Raman intensities are predicted to monotonically increase as resonance excitation is approached. In contrast, the observed resonance and preresonance Raman intensities can decrease as excitation approaches resonance if the sample contains absorbing impurities or chromophores that do not enhance the analyte Raman bands. For resonance excitation (defined to occur for excitation within two standard deviations of the analyte Gaussian absorption maximum), a minimum in the EFDORI requires (1) that the impurity absorption band be at least $(2^{1/2})/2$ narrower than the analyte absorption band, and (2) that the frequency offset between analyte and impurity absorption maxima be $<2\sigma_a(1 - 2(\sigma_i/\sigma_a)^2)$.

Thus, conditions for a decrease in the observed resonance Raman intensity with excitation closer to resonance will be rare. Spectral S/N maxima will typically occur with resonance excitation. Decreasing observed preresonance Raman intensities and normal Raman intensities can occur in the presence of impurity absorption.

ACKNOWLEDGMENT

We thank Dr. Sergei Bykov for his helpful discussions. This work was supported by ONR contract N00014-12-1-0021.

1. D.A. Long. The Raman Effect: a Unified Treatment of the Theory of Raman Scattering by Molecules. West Sussex, UK: John Wiley and Sons Ltd., 2002.
2. R.L. McCreery. Raman Spectroscopy for Chemical Analysis. New York: John Wiley and Sons Ltd., 2000.
3. S.A. Asher. "UV Resonance Raman Studies of Molecular Structure and Dynamics: Applications in Physical and Biophysical Chemistry". Ann. Rev. Phys. Chem. 1988. 39(1): 537-588.
4. S.A. Oladepo, K. Xiong, Z. Hong, S.A. Asher, J. Handen, I.K. Lednev. "UV Resonance Raman Investigations of Peptide and Protein Structure and Dynamics". Chem. Rev. 2012. 112(5): 2604-2628.
5. C.M. Jones, S.A. Asher. "Ultraviolet Resonance Raman Study of the Pyrene S4, S3, and S2 Excited Electronic States". J. Chem. Phys. 1988. 89(5): 2649-2661.
6. D.F. Shriver, J.B.R. Dunn. "The Backscattering Geometry for Raman Spectroscopy of Colored Materials". Appl. Spectrosc. 1974. 28(4): 319-323.
7. T.C. Strekas, D.H. Adams, A. Packer, T.G. Spiro. "Absorption Corrections and Concentration Optimization for Absorbing Samples in Resonance Raman Spectroscopy". Appl. Spectrosc. 1974. 28(4): 324-327.
8. C. Liu, R.W. Berg. "Nonlinearity in Intensity versus Concentration Dependence for the Deep UV Resonance Raman Spectra of Toluene and Heptane". Appl. Spectrosc. Rev. 2012. 48(5): 425-437.
9. L.S. Greek, H.G. Schulze, C.A. Haynes, M.W. Blades, R.F.B. Turner. "Rational Design of Fiber-Optic Probes for Visible and Pulsed-Ultraviolet Resonance Raman Spectroscopy". Appl. Opt. 1996. 35(21): 4086-4095.
10. L.S. Greek, H.G. Schulze, M.W. Blades, C.A. Haynes, K.-F. Klein, R.F.B. Turner. "Fiber-Optic Probes with Improved Excitation and Collection Efficiency for Deep-UV Raman and Resonance Raman Spectroscopy". Appl. Opt. 1998. 37(1): 170-180.
11. A.C. Albrecht, M.C. Hutley. "On the Dependence of Vibrational Raman Intensity on the Wavelength of Incident Light". J. Chem. Phys. 1971. 55(9): 4438-4443.
12. A.C. Albrecht. "On the Theory of Raman Intensities". J. Chem. Phys. 1961. 34(5): 1476-1484.
13. D.D. Tuschel, A.V. Mikhonin, B.E. Lemoff, S.A. Asher. "Deep Ultraviolet Resonance Raman Excitation Enables Explosives Detection". Appl. Spectrosc. 2010. 64(4): 425-432.
14. J.M. Dudik, C.R. Johnson, S.A. Asher. "Wavelength Dependence of the Preresonance Raman Cross Sections of CH_3CN, SO_4^{2-}, ClO_4^-, and NO_3^-". J. Chem. Phys. 1985. 82(4): 1732-1740.
15. M. Ghosh, L. Wang, S.A. Asher. "Deep-Ultraviolet Resonance Raman Excitation Profiles of NH_4NO_3, PETN, TNT, HMX, and RDX". Appl. Spectrosc. 2012. 66(9): 1013-1021.
16. J. Friedman, R.M. Hochstrasser. "Interference Effects in Resonance Raman Spectroscopy". Chem. Phys. Lett. 1975. 32(3): 414-419.
17. P. Stein, V. Miskowski, W.H. Woodruff, J.P. Griffin, K.G. Werner, B.P. Gaber, T.G. Spiro. "Raman Antiresonance: Deenhancement of Raman Intensity by Forbidden Electronic Transitions". J. Chem. Phys. 1976. 64(5): 2159-2167.